PAPER • **OPEN ACCESS**

Green synthesis of gold nanoparticles: pros and cons of natural compounds

To cite this article: Caterina Medeot *et al* 2024 *Nano Ex.* **5** 045020

NANO EXPRESS

OPEN ACCESS

RECEIVED
5 September 2024

REVISED
20 November 2024

ACCEPTED FOR PUBLICATION
16 December 2024

PUBLISHED
26 December 2024

PAPER

Green synthesis of gold nanoparticles: pros and cons of natural compounds

Caterina Medeot[1,2], Ahmed Alsadig[2,8], Francesco D'Amico[3], Roberto Costantini[4,5], Claudio Lentini Campallegio[4], Albano Cossaro[5,6], Hendrik Vondracek[3,9], Giovanni Birarda[3], Paola Posocco[7], Pietro Parisse[2,5], Loredana Casalis[2,10,*] and Serena Bonin[1,10,*]

[1] DSM—Department of Medical Sciences, University of Trieste, 34149 Trieste, Italy
[2] NanoInnovation Lab, Elettra Sincrotrone Trieste S.C.p.A., 34149 Trieste, Italy
[3] Elettra-Sincrotrone Trieste S.C.p.A., Area Science Park, 34149 Trieste, Italy
[4] DF—Department of Physics, University of Trieste, 34127 Trieste, Italy
[5] Istituto Officina dei Materiali - National Research Council (CNR-IOM), Area Science Park, 34149 Trieste, Italy
[6] Department of Chemical and Pharmaceutical Sciences, University of Trieste, Trieste, 34127, Italy
[7] Department of Architecture and Engineering (DEA), University of Trieste, 34127 Trieste, Italy
[8] Current address: Institute of Radiopharmaceutical Cancer Research, Helmholtz-Zentrum DresdenRossendorf, Bautzner Landstraße 400, 01328, Dresden, Germany.
[9] Current address: Diamond Light Source Ltd, Harwell Science and Innovation Campus, Didcot, Oxfordshire OX11 0DE, UK.
[10] Co-last authors.
[*] Authors to whom any correspondence should be addressed.

E-mail: loredana.casalis@elettra.eu **and** sbonin@units.it

Keywords: gold nanoparticles, green synthesis, cocoa powder, flavonoids

Supplementary material for this article is available online

Abstract

Gold nanoparticles (AuNPs) have attracted scientific interest for their unique properties and diverse applications, across biomedical fields, including sensing, diagnostics, and therapeutic interventions. However, standard wet chemistry synthetic methods for particles synthesis bare limitations, particularly in separating AuNPs from the reaction mixture. Therefore, there is a growing demand for environmentally friendly synthesis routes that minimize waste and utilize non-toxic solvents. Despite advances in this field, many current studies lack standardized protocols, and the underlying mechanisms of the reducing reaction remain unclear. Through comprehensive spectroscopic and morphological analyses, we investigated the redox reactions involved in AuNP formation with various natural extracts, aiming to establish an optimized protocol for producing small, spherical, and monodisperse AuNPs. Our findings demonstrate that cocoa powder extract effectively yields reproducible, spherical AuNPs with a diameter of 11 nm. Comparative analysis with single cocoa powder molecular components identified catechins, a class of flavonoids, as the primary reducing agent in green AuNP synthesis. Catechins also form a protective layer around the AuNPs. However, the simultaneous, unavoidable presence of this layer implemented with fatty acids and proteins, although fundamental for colloidal stability, limits further functionalization of the AuNPs, highlighting a trade-off between stability and functional versatility.

1. Introduction

Metallic nanoparticles have gained enormous scientific and technological interest due to their large surface-to-volume ratio, small size, and intriguing optical/thermal/electrical characteristics [1–3]. Owing to their unique properties, such as stability, biocompatibility, low toxicity, and chemical inertness, gold nanoparticles (AuNPs), in particular, have attracted the highest attention [4] as drug delivery system prior suitable functionalization [5]. However, effective *in vivo* application of AuNPs requires monodispersion and specific dimension, below 20 nm, in order to overcome the biochemical barrier in the body [6].

Routinely, AuNPs are synthesized via bottom-up approaches by reducing cationic Au(III) with a specific reducing agent, followed by a stabilization with a capping agent to prevent particle aggregation. The classical method introduced by Turkevich *et al* in 1951, remains one of the widely used approach to produce monodisperse AuNPs, using trisodium citrate as a reducing and stabilizing agent [7]. By adjusting the citrate concentration and its ratio to gold salt, particle sizes can be controlled, achieving colloidal AuNPs in the range of 20 nm or below. Citrate-capped AuNPs are particularly favorable for functionalization protocols, as ligand exchange procedure allows for the replacement of citrate with desired functional groups. For example, in the work of Deka *et al* AuNPs were conjugated to DNA strands to assess helicase activity [8]. Specifically for drug delivery, S. Aryal and co-workers conjugated doxorubicin to AuNPs as anticancer carriers [9].

Despite the feasibility of classical chemical methods for synthesizing AuNPs, their limitations reside in the difficulty of being separate from their reaction mixture, which in some cases may contain toxic chemicals and organic solvents such as toluene [10]. Such considerations resulted in several reports proposing novel environmentally-friendly routes for synthesizing AuNPs based on green chemistry [11], which prioritize uses of safer solvents (i.e. water) [12]. In this regard, plant-based extracts are desirable as they bring crucial synergy between nanotechnology tools and plant sciences, and could be potentially scaled-up to large production [13], maintaining low temperatures/pressures, and, most important, minimizing chemical wastes [14]. Up to now, AuNPs green synthesis has been achieved by using various plants, such as *Aloe vera* plant extracts [15] and black tea leaf extracts [16] and even from microorganisms, such as bacteria like *Pseudomonas aeruginosa* [17] or fungi (Candida Albicans [18]) [19], as well as other biological sources as enzymes and cell lines [20]. However, most of the studies in this area lack standardized synthesis procedures. More importantly, the nature of the reaction and the roles of specific extract constituents in the colloidal synthesis are still unknown. Moreover, the potential for functionalization comparable to citrate-capped AuNPs, is still limited and challenging, as the natural stabilizing layer formed during green synthesis imposes constraints on further modifications.

This study aims to compare various readily available natural extracts as reducing agent for Au(III) to synthesize AuNPs under mild conditions without the use of any other chemical. Based on literature research, we selected lemon juice [21], tea leaves [22], coffee [23], and cocoa powders [24] due to their commercial availability and potential for one-step synthesis. Thorough spectroscopic and morphological analyses was performed to elucidate the nature of the redox mechanism driving the AuNPs formation and to identify the most reproducible protocol to producing clean, shape-controlled, and monodisperse AuNPs with dimensions less than 20 nm. The stability of these AuNPs in physiological media was also assessed, as these is essential conditions to move into further biological applications.

2. Experimental section

2.1. Materials

Lemons, commercial tea (Twining's© Pure green tea), coffee (Illy© blend 100% arabica ground coffee), and cocoa powder (Mondo Natura©) were purchased from local markets in Trieste, Italy. Gold (III) chloride solution, 1,3,7–dimethylxanthine (caffeine), 3,7–dimethylxanthine (theobromine), catechin, oxalic acid, quercetin, and 11-mercaptoundecanoic acid (MUA) were purchased from Sigma-Aldrich Chemical Co. (St. Louis, MO, USA). Coomassie Brilliant Blue G-250 (Bradford solution for protein determination was purchased from Bio-Rad Laboratories (Hercules, CA, USA). 1 (mercaptoundec-11-yl)hexa(ethylene glycol) ($SH\text{-}(CH_2)_{11}\text{-}EG_3OH$), for brevity TOEG3, was purchased from Prochimia Surfaces (Gdynia, Poland).

2.2. Preparation of AuNPs

Synthesis procedures reported in [21–24] were adapted to cocoa powder protocol for comparable methods. Specifically, natural extracts (i.e., coffee powder, tea bags and cocoa powder) were prepared using 125 mg of powder or leaves in 50 mL of milli-Q water, mixed for 15 min on a magnetic stirrer plate. For lemon, 1.1 mL of juice was diluted with 48.9 mL of milli-Q water. The extracts were then purified with a 0.45 μm syringe filter and mixed with varying concentrations of gold chloride, as detailed in table 1, before being brought to boil under magnetic stirring. The reaction was maintained at boiling for 30 min to ensure the complete reduction of the gold salt, then allowed to cool down to room temperature. Additional syntheses were conducted as follows: caffeine and Theobromine syntheses was first performed according to the work of Reena et *al* [25]. Egg yolk-based synthesis was performed according to the protocol by Nadaroglu and coworkers [26]. Synthesis with catechin was adapted from Choi *et al* [27] to use the same gold chloride concentration and the same volume of water as in the other syntheses. Quercetin synthesis was conducted by adding 0.5 mM of gold chloride to a 0.28 mM extract solution. Last, 1 mM of the oxalic acid extract was used to synthesize nanoparticles in a final volume of 50 mL of milli-Q water and 0.5 mM of gold chloride. Prior to spectroscopic and microscopic measurements, samples were diluted 1:10 with milli-Q water.

Table 1. Summary of the natural extracts used in AuNPs synthesis, the quantities of each extract, and the corresponding gold chloride concentrations. For successful synthesis, the maximum absorption wavelength is also reported. Citrate-capped synthesis conditions are also shown for comparison.

Source	Extract (mg)	$HAuCl_4$ (mM)	λ_{max} (nm)
Cocoa	125	0.5	530 nm
	125	0.05	
	12.5	0.5	
	1250	0.5	
Coffee	125	0.5	
	125	2	
Tea	125	0.5	540 nm
	125	1	
Lemon	125 (1 ml*)	0.5	
	125 (1 ml*)	1	

2.3. Microscopic and spectroscopic characterization of AuNPs

AuNPs morphology was verified by Transmission Electron Microscopy (TEM) (Philips EM 208) equipped with an acquisition system Camera OLYMPUS QUEMESA, Software RADIUS (EMSIS electron microscopy imaging company, Muenster, Germany). The average size distribution of the resulting nanoparticles was determined through Fiji software by setting a mask in the range of 50–110 nm^2. The aspect ratio of particles, in the range 0–1 where 1 is a perfect circle and values closer to 0 indicate a more irregular shapes, was calculated as described by the following equation:

$$AR = \frac{Minor\ axis}{Major\ axis}$$

measuring the length of the two axes with Fiji software. The aspect ratio (AR) is defined as the ratio of the width (or shorter dimension) to the height (or longer dimension) of an object. For each type of particles 70 single colloids were analyzed.

Atomic Force Microscopy (AFM) (Solver Pro, NT-MTD, Moscow, Russia instrument) performed at the NanoInnovation Laboratory-Elettra-Sincrotrone S.C.p.A Trieste was used to investigate NPs distribution and their average height. The analysis was performed with NSG36 probe tip, set point 5,000 in semi-contact mode with 1,00 gain. The investigated areas were $30 \times 30\ \mu m^2$, $10 \times 10\ \mu m^2$, and $3 \times 3\ \mu m^2$ achieved with a resolution of 512 points and a scan rate of 1,0000 Hz. AFM images were analyzed by Gwyddion software. Images were processed and the AuNPs average height was determined by creating a mask with the command '*mask grains by threshold*' selecting all the values higher than the expected dimensions according to the intensity levels of the image. Through the command '*Distributions of grains*' the raw values of 'maximum value' and 'equivalent disc radius' were exported, corresponding to the height and the radius of each particles analyzed. Data were then imported into OriginLab software for statistical analysis. Data were plotted as histogram and fitted with 'multipeak fitting' with Gaussian model.

Hydrodynamic diameter and zeta potential readouts were obtained by Dynamic Light Scattering (DLS) (Zetasizer Nano, Malvern Instrument, UK) in a disposable microcuvette. UV–visible spectroscopic measurements were carried out in the wavelength range of 200–800 nm (Perkin-Elmer, lambda 25, Waltham, MA, USA). UV Resonant Raman (UVRR) experiments were carried out at the IUVS beamline in Elettra-Sincrotrone Trieste. Measurements were performed using a 266 nm laser as the excitation source in a backscattering configuration. Diffused Raman signal was collected and dispersed through a single-stage Czerny–Turner spectrometer (Andor) with 750 mm of focal length, equipped with 1800 lines/mm holographic reflection grating, 250 nm ruled. The laser beam power reaching the sample was approximately 0.1 mW. The spectral resolution was near 8 cm^{-1}. Fourier Transform Infrared Attenuated Total Reflection (FTIR-ATR) measurements were performed at SISSI-Bio beamline at Elettra Sincrotrone Trieste, using a VERTEX 70 interferometer (Bruker Optics, Billerica MA, US) equipped with a single reflection ATR accessory with a diamond crystal (MIRacle Pike, Madison WI, US). Repeted spectra were acquired with a scanner speed of 5 kHz. XPS measurements were performed at the Anchor-Sundyn laboratory of the ALOISA beamline of Elettra Synchrotron [28], using a monochromatized Al Kα x-ray source (Omicron XM 1000) and a 150 mm Hemispheric Analyzer (Specs) operated with $E_{pass} = 50$ eV. The overall resolution was 0.6 eV.

2.4. Biochemical characterization of the samples

Bradford assay was carried out to estimate the protein concentration in natural extracts and synthesized AuNPs. Measurements were performed using a spectrophotometer TECAN infinite F200 PRO (Tecan Trading AG, Switzerland) at 595 nm. The protein amount was determined using a 0.1–1 mg mL^{-1} BSA calibration curve. Each sample was analyzed in triplicate [29].

2.5. Functionalization protocol

Cocoa AuNPs and citrate-capped AuNPs, used as reference model, were functionalized by forming a mixed self-assembled monolayer (mixed-SAM) with MUA and TOEG3. TOEG3, a pegylated alkane thiol, acts as a spacer to passivate the surface and properly direct associated linkers. Both particles were centrifuged at 14,462 × g up to the complete formation of a pellet. The supernatant was discarded, and NPs resuspended in a 30:70% (v/v) solution of MUA and TOEG3 at scalar concentrations (1 μM, 2 μM, 3 μM, 4 μM, 5 μM, 10 μM), and incubated overnight. The following day, UV–vis analysis was carried out to assess the extent of ligand-exchange. After that, the solution was centrifuged again at 14,462 × g to remove any unbound ligands, the supernatant was discarded, and the pellet was resuspended in 100 μL of milli Q-water, for further characterization.

3. Results and discussion

3.1. Synthesis of the AuNPs

In this study, we analyzed a panel of four food extracts starting from the literature review [25–28], slightly modifying the synthesis protocols to guarantee comparable procedures among the different extracts. Concentrations used are reported in table 1. For lemon juice extract, AuNPs consistently aggregated at all concentrations tested. The solution color turned to black, and the UV–vis spectrum exhibited an aggregation peak around 600 nm. For coffee powder, no color change was observed at either concentration, indicating a failure in the AuNPs synthesis. However, the formation of AuNPs was evident when tea or cocoa extracts were used. In the case of tea extract, at a 1.0 mM concentration of $HAuCl_4$, the solution color turned to dark purple, pointing to high-size aggregates. Moreover, impurities remained in the reaction mixture even after filtration. At variance, using cocoa extract, with 125 mg of cocoa powder and 0.5 mM $HAuCl_4$, resulted in successful synthesis of AuNPs. The solution color changed from pale brown to dark red, suggesting the formation of colloidal AuNPs. The maximum adsorption peak observed in the UV–vis spectroscopy was 530 nm, indicating that the AuNPs were smaller than those obtained using tea extract. Several other relative concentrations of cocoa powder and $HAuCl_4$ (as reported in table 1) were tested, to optimize the synthesis aiming to obtain a more monodispersed batch of cocoa-based AuNPs (CAuNPs). In details, from 1250 mg of cocoa powder and 0.5 mM of $HAuCl_4$, or 125 mg of cocoa and 0.05 mM $HAuCl_4$ resulted in no particle formation. In addition, the use of 12.5 mg of cocoa and 0.05 mM of $HAuCl_4$ produced incomplete nanoparticle synthesis, with residual gold chloride indicating insufficient reduction. Therefore, we can conclude that the optimal conditions for green AuNPs synthesis are 125 mg cocoa powder with 0.5 mM of $HAuCl_4$. Under these conditions, we successfully obtained spherical AuNPs, with acceptable monodispersity and sizes below 20 nm, through a one-step synthesis.

3.2. Morphological characterization

The size and morphology of CAuNPs were characterized using TEM, DLS, and AFM. TEM analysis (figure 1(a)) revealed an average size distribution of 10.7 ± 3.1 nm with a spherical shape. Aspect ratio (AR) analysis was carried out to estimate the approximately particles' sphericity. An average AR of 0.92 ± 0.06 was retrieved for CAuNPs confirming the spherical morphology of the AuNPs. TEM images of CAuNPs revealed the presence of a coating layer surrounding the particles. While the presence of such a shell around green AuNPs has been reported in other studies [16, 24, 30], a plausible explanation about its composition and nature of this coating remains unclear within the scientific literature.

The presence of the coating layer was also confirmed by DLS as an enlarged size distribution. In fact, a bimodal distribution of CAuNPs size was measured, with a main average hydrodynamic diameter at 48.2 ± 12.9 nm, and a second broader peak at 187.2 ± 62.5 nm. Concurrently, a zeta potential of −28.6 ± 3.9 mV was measured, confirming the stability of the synthesized AuNPs.

To extend the value of TEM data to a more natural environment (i.e., air, liquid solution) AFM imaging was used to investigate the height of the colloids. AFM morphological analysis was performed from typical images as the one in figure 1(c). From the particle analysis we can extract a bimodal size distribution, with the main average height peaked at 9.6 ± 0.1 nm and a second, slightly broader one at 19.8 ± 20.8 nm, pointing to the possible presence of aggregates, although much smaller than in the DLS. The error in the statistical analysis is represented by mean and standard deviation of the single peaks from the Gaussian fit.

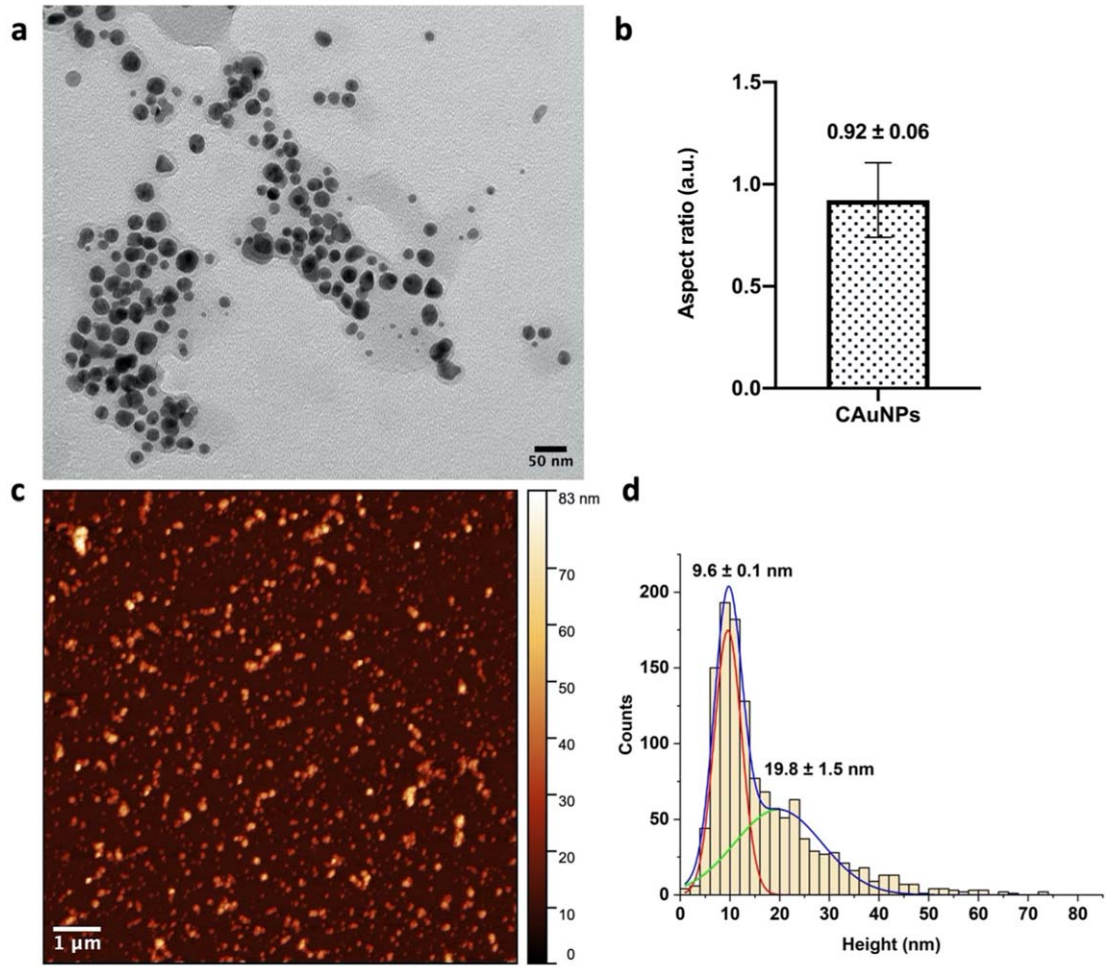

Figure 1. (a) Representative TEM image of CAuNPs. (b) Statistical analysis representing the average AR for CAuNPs. (c) Representative AFM image of CAuNPs. (d) AFM height distribution with a double-gaussian fit. Scale bars are reported.

The discrepancy in the average size of CAuNPs retrieved from the three approaches arises from the differences in the principles of the techniques. DLS, a scattering technique, is highly sensitive to aggregations or to dust particles. For this, it is reasonable that the laser simultaneously measures two or more particles. In addition, previous findings have shown that flavonoids tend to aggregate when measured with DLS, potentially leading to false bioassay results [31]. Also, the coating of flavonoids provides a consistence increase in the average hydrodynamic diameter [32]. On the other hand, TEM measurements are performed in vacuum condition and particles are spread over the support grid. The resolution of TEM is about 1 nm or better, therefore at higher magnification is it possible to distinguish laterally overlapped particles and measure them as single. However, TEM measures the 2D, surface-projected profile of the particles. On the contrary, AFM can distinguish particle's 3D profile, when deposited on a surface. AFM resolution is highest in the vertical direction, which defines particle's height ($<$1 nm). Thus, the two main peaks shown in figure 1(d) represent single particles (9.6 ± 0.1 nm) and vertically overlapping particles (19.8 ± 20.8 nm), respectively. We highlight here how this integrated, multi-technique morphological analysis offered valuable insights into the characteristics of CAuNPs. Next, we concentrated on identifying the most relevant molecules present in the cocoa extract, and their role on nanoparticles synthesis. Based on the literature, key components such as caffeine derivatives (e.g., theobromine), flavonoids (e.g., catechins and quercetin), oxalates (e.g., oxalic acid), fatty acids, and proteins [33, 34] are reported as key components. To investigate the role of each molecule as a potential reducing agent/stabilizer in the formation of CAuNPs, AuNPs were synthetized by gold chloride to single cacao extract key components in the amounts reported in table 2. For each component, the correct amounts of gold chloride was established starting from reference protocols (reported in table 2), and correlated to the protocol used for the synthesis of cocoa AuNPs [24]. A comprehensive chemical characterization of both the extract alone and the synthesized AuNPs was conducted via a careful UV–vis, UVRR, ATR-FTIR, and XPS spectroscopy analysis.

Table 2. Summary of cocoa extract components, the amount used to synthesize AuNPs, and the correspondent gold chloride concentration. Caffeine and theobromine were considered for caffeine derivatives. As flavonoids, catechin, and quercetin were analyzed. Oxalic acid instead for oxalates groups. Lastly, egg yolk was used as a possible source of proteins. For the successful synthesis, maximum absorption wavelength is also reported. Respective references are reported.

Component	Extract (mg or mM)	$HAuCl_4$ (mM)	λ_{max} (nm)	References
Caffeine	0.5 mM	0.5		[24]
	125 mg	1		
Theobromine	0.5 mM	0.5		
	125 mg	100		
Catechin	0.5 mM	0.5	539 nm	[26]
Quercetin	0.5 mM	0.5		
Oxalic acid	1 mM	0.5		
Egg yolk	1 ml	10		[28]

3.3. Synthesis and characterization of catechin-capped AuNPs

Among the key components of cocoa extract, only catechin enabled the successful synthesis of AuNPs, identifying it as the main agent in CAuNP formation. UV–vis analysis displayed a maximum absorption peak at 539 nm (figure 3(S) (a) in the supplementary materials). TEM analysis revealed an average size distribution of 36.4 ± 8.8 nm, larger than the CAuNPs, with spherical morphology and in the presence of a coating shell. The average particle height measured by AFM (figure 3(S)(b) in the supplementary material), was 48.3 ± 7.4 nm. DLS measurements yielded an average diameter of 80.7 ± 51.6 nm, showing, as in the case of CAuNPs, higher values than expected. The zeta-potential value measured -29.1 ± 8.5 mV.

The ability of synthetizing AuNPs from catechins-enriched solutions supports to the hypothesis of the relevant role played by flavonoids as gold reduction agents in cocoa extracts. In details, as shown by our data, both CAuNPs and catechin-capped AuNPs had an altered hydrodynamic diameters in DLS measurements. Pohjala and Tammela previously reported an aggregating behavior in phenolic compounds, particularly flavonoids, at higher concentrations when analyzed by DLS, leading to false bioassay results [31]. From the literature, cocoa powder, seems to contain a high content of catechins per serving, in the range of 81.40–447.62 $\mu g\, g^{-1}$ in commercial products [34]. Therefore, it is reasonable to associate the bimodal distribution and the higher hydrodynamic diameter obtained by DLS analysis on catechin-capped AuNPs and CAuNPs to flavonoids aggregating tendency.

3.4. Spectroscopic characterization

To shed light on the chemical origin of the observed particle coating layer, an extensive spectroscopic analysis was performed. The absorption spectrum of cocoa extract was compared with the molar extinction coefficients of the expected components, as depicted in figure 2. The cocoa extract spectrum is marked by an absorption peak at 273 nm and a strong absorption tail below 250 nm. In details, line-shape similarities between cocoa extracts spectrum and those of caffeine, theobromine, and catechin can be appreciated, while quercetin and oxalic acid show a non-matching absorption fingerprint. Notably, catechin exhibits a characteristic absorption peak at ≈278 nm [34–37]. The measured spectra also align with the presence of proteins in the extract, as protein typically display a broad peak at 280 nm and a substantial increase of absorbance below 230 nm [37]. To quantify the proteins concentration in the solution, Bradford assays was carried out, confirming the presence of 0.10–0.11 $mg\, mL^{-1}$ protein concentration in both the cocoa extract and the CAuNPs solution.

To gain further insights, vibrational spectroscopy (ATR-FTIR and UV Resonant Raman) measurements were carried out, with the corresponding spectra shown in figure 3. The ATR-FTIR spectra of drop casted-cocoa extract at high energy show three specific peaks at 2925 cm^{-1}, 2855 cm^{-1}, and 1745 cm^{-1}, absent in both catechin and theobromine solutions, which can be considered as a fingerprint of the fatty acid presence (symmetric and asymmetric stretching vibrations of aliphatic CH_2 groups, plus triglycerides ester carbonyls) [38, 39]. The similarity between cocoa extract and catechin solution appears also from the ATR-FTIR spectra in the 600–1900 cm^{-1} range: peaks at 1610 cm^{-1}, 1519 cm^{-1}, 1146 cm^{-1}, and 1030 cm^{-1}, absent in the theobromine spectrum (figure 3(a)). The presence of proteins, already confirmed by Bradford assay, aligns with the amide-I and amide-II bands in the FTIR spectra, at ≈1650 cm^{-1} and ≈1550 cm^{-1} [40], respectively. We further observed that in CAuNPs, the presence of catechin, proteins, and fatty acids was increased. It is possible

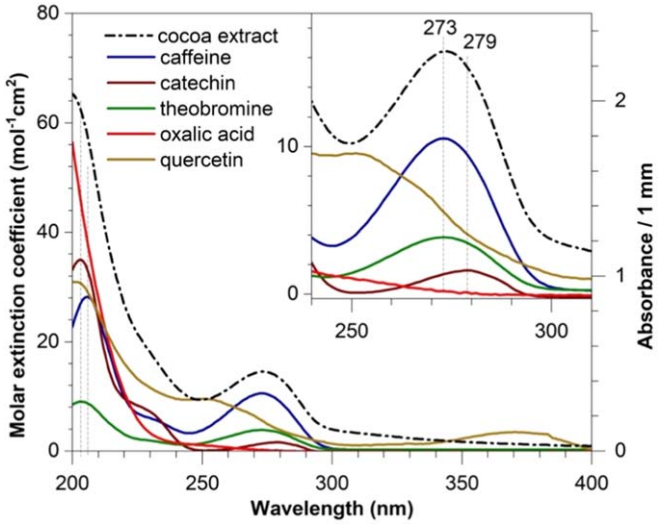

Figure 2. UV-visible absorption spectra of theobromine, caffeine, catechin, quercetin and oxalic acid molar extinction coefficients in the wavelength range of 200–800 nm. Cocoa extract spectrum is reported as reference.

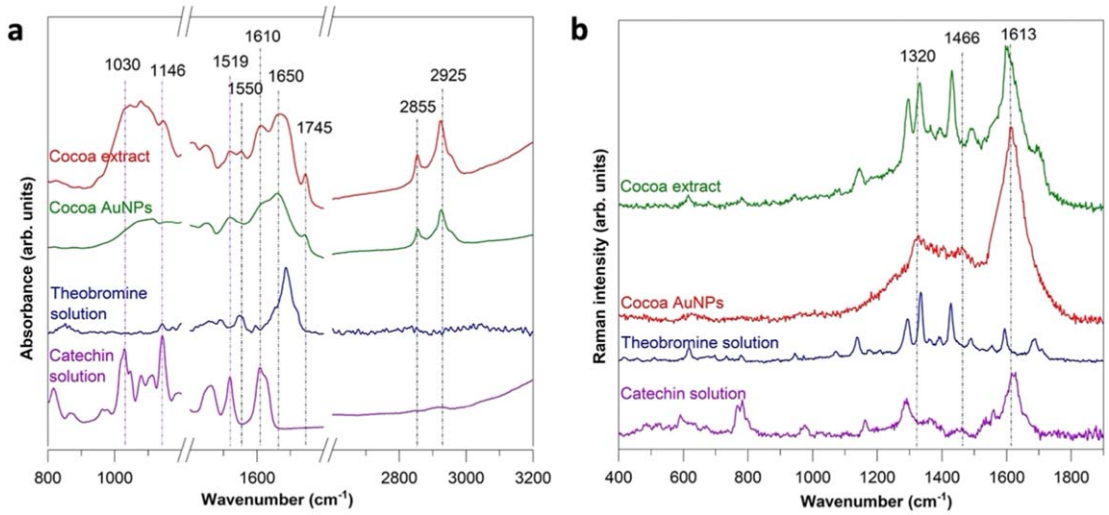

Figure 3. (a) ATR-FTIR spectrum of cocoa AuNPs, cocoa extract and theobromine/catechin solutions respectively in the wavenumber range of 600–1900 cm^{-1} and 2700–3700 cm^{-1}. (b) UVRR spectra collected at $\lambda_{exc.}$ = 266 nm of cocoa AuNPs, cocoa extract and theobromine/catechin solutions respectively, both in drop and drop-casted. The spectra of theobromine aqueous solution, and catechin, are shown for comparison.

that catechin, which is easily oxidized, promotes protein precipitation on the surface of the AuNPs. UVRR spectra (figure 3(b)), collected at 266 nm, support this hypothesis. The intense, broad peak observed at 1610 cm^{-1}, can be associated with catechin derivatives. However, peaks at 1320 cm^{-1}, 1466 cm^{-1} and 1613 cm^{-1} might point to the presence of theobromine. However, the presence of an intense peak at 1613 cm^{-1}, characteristic of catechin, was also found on the NPs surface. The lack of a complete correspondence between pure catechin peaks supports a chemical modification of catechins after the synthesis reaction. Tables 4 and 5 supplementary materials reported a summary of peak assignation for ATR-FTIR and Raman analysis.

XPS measurements were also carried out, to investigate the chemical constitution of these organic residues and synthetized AuNPs to identify the presence of radicals. Representative XPS spectra collected on cocoa extract, catechin, theobromine solutions, and CAuNPs, all deposited by drop casting on an Au(111) surface, are displayed in figure 4. To simplify the peak attribution, we also measured XPS spectra of catechin- synthesized AuNPs. We assigned most of the peaks referring to a previous work of Rouxhet et *al* [41]. Regarding cocoa extract, the analysis of the broad C 1 s photoemission curve shows a first peak at 284.33 eV, which indicates the presence of C–C and C–H bonds and is compatible with the coexistence of aliphatic chains, typical of fatty acids molecules. Also peaks at 287.6 eV and 289.1 eV, assigned respectively to C=O and COO- groups, are

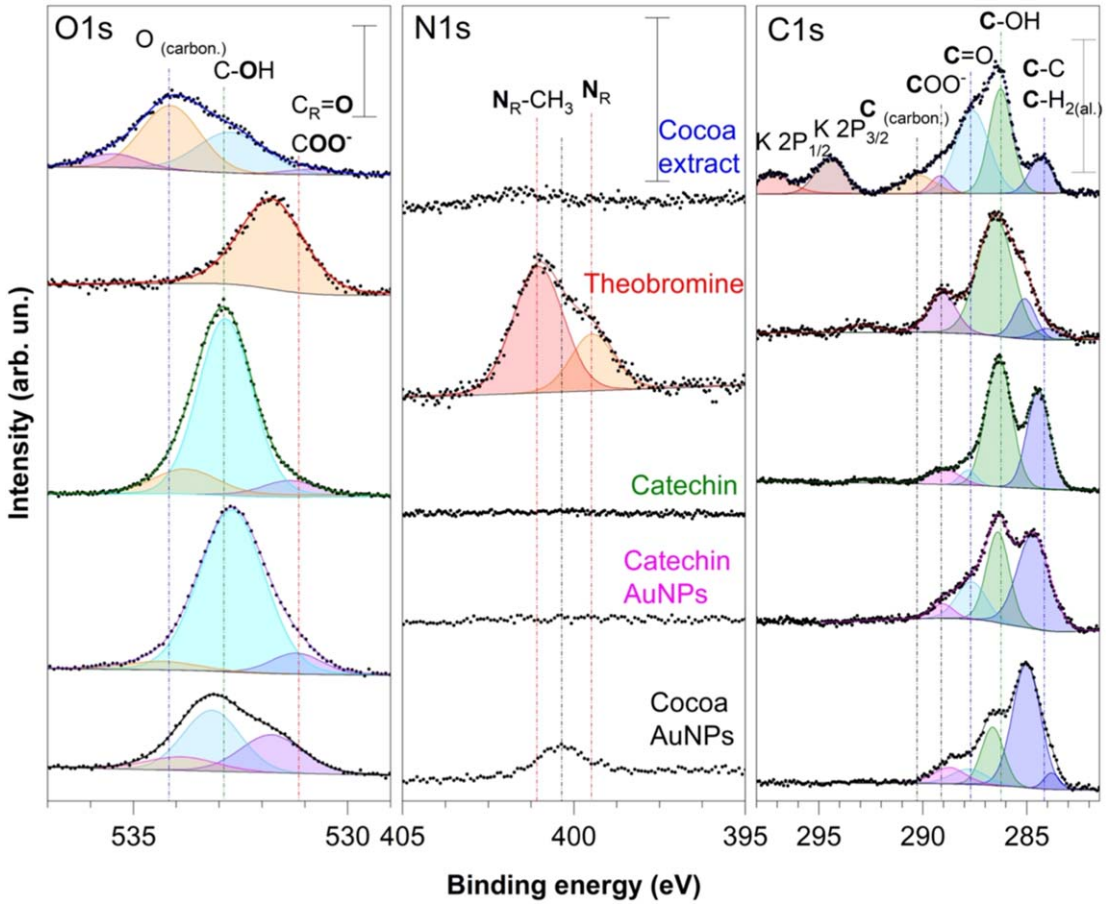

Figure 4. XPS spectra collected on cocoa extract, theobromine, catechin, catechin AuNPs, and cocoa AuNPs deposited by drop-casting on Au(111) surface.

characteristics of fatty acids, as well as oxalate carboxylic groups. The peak at 286.3 eV instead, can be assigned to the flavonoid hydroxyl groups, already detected by FTIR measurements. The O 1 s peak analysis was made by using four components: a small one at 530.9 eV, due to the COO− contribution, and two other peaks at 532.7 eV and 534.1 eV, which can be assigned respectively to hydroxyls and COOH groups. A further weak peak can be assign to the carboxylic C=O and OH oxygen atoms [39]. Lastly, another weak component at 535.5 eV, can be reasonably attributed to food preservative carbonates. As expected, the N 1 s XPS spectrum only shows some faint features of difficult assignment. Overall, the cocoa extract solution has much more affinities with the catechin solution than with the theobromine one, in agreement with our previous vibrational spectroscopy results. In particular, the C 1 s catechin peak deconvolution allows the identification of four chemical shifted components, respectively at 284.44, 286.35, 287.85, and 289.1 eV, close in energy to the ones derived from cocoa C 1 s peak fit. The component at 286.35 eV can be assigned to the five C–OH carbon atoms of the catechin molecule, while the further nine C atoms to the 284.44 eV peak. The peaks at 287.85 eV (C=O) and 289.1 eV (COO−) instead, constituting less than 15% of the total carbon atoms, can be assigned to oxidized and/or radical forms of catechins. Regarding the O 1 s peak, three components have been found, respectively at 531.2 eV, 532.7, and 534.0 eV. The first component can be assigned to C=O oxygen atoms and confirms, as seen from the C 1 s peak analysis, that a small fraction of catechins is oxidized. The peaks at 532.7 eV and 534.0 eV instead can be assigned respectively to the hydroxyl's oxygen atoms and to the remaining oxygen of the catechin rings.

In the case of catechin AuNPs, in the C 1 s peak we identified the same components detected in pure catechin, respectively at 284.69 eV, 286.38 eV, 287.7 eV, and 289.1 eV. Interestingly, the peak area relative to the C–OH atoms decreased in catechin AuNPs, while the low energy peak area increased. All these spectral modifications are compatible with an oxidation reaction of catechin molecules during NPs synthesis. This is also supported by the O 1 s peak line shape modification. A similar oxidation process of catechins in cocoa extract during the CAuNPs synthesis can be inferred by spectra analogies. Table 3 provides a detailed summary of peaks assignation for XPS analysis.

Our results support an oxidation of the original catechin compounds upon AuNPs synthesis reaction, confirming its role as a reducing agent in the synthesis of gold nanoparticles. In detail, catechins are composed of

Table 3. Summary table of peaks assignation in XPS analysis for the considered systems.

		Position (eV)	Area (%)	Width (eV)	Assignation
Cocoa Extract	C1s	284.33 ± 0.03	11.7 ± 0.3	1.26 ± 0.07	C–C/C–H
		286.3 ± 0.1	39.8 ± 1.1	1.34 ± 0.12	C–OH
		287.6 ± 0.2	30.5 ± 3.6	1.5 ± 1.0	C=O
		289.1 ± 0.8	13.3 ± 3.1	1.6 ± 1.3	COO^-/K_2CO_3
		290.6 ± 0.9	4.5 ± 0.9	1.4 ± 1.0	$KHCO_3$
	K 2p	294.48 ± 0.02	60.7 ± 9.7	1.60 ± 0.08	Carbonates K $2p_{3/2}$
		297.19 ± 0.05	39.2 ± 4.9	2.0 ± 0.3	Carbonates K $2p_{1/2}$
	O 1 s	530.9 ± 0.7	3.6 ± 0.1	1.4 ± 1.0	COO^-
		532.7 ± 1.1	36.9 ± 0.9	1.9 ± 1.5	C-=O(–OH)
		534.1 ± 0.2	49.7 ± 1.1	1.6 ± 1.4	C=O=C–O(–OH)
		535.5 ± 1.4	9.7 ± 0.6	1.5 ± 1.2	Carbonates
Theobromine	C1s	284.0 ± 1.1	4.8 ± 0.2	1.5 ± 1.3	C–C
		285.1 ± 0.1	13.5 ± 0.3	1.2 ± 0.6	C–C
		286.5 ± 0.1	64.9 ± 0.3	2.00 ± 0.16	C–N
		289.05 ± 0.05	16.8 ± 0.6	1.6 ± 0.2	N-(C=O)–N
	O1s	531.79 ± 0.01	100*	1.80 ± 0.02	N-(C=O)–N
	N1s	399.46 ± 0.07	27.8 ± 0.4	1.50 ± 0.13	
		401.04 ± 0.04	72.2 ± 0.4	1.73 ± 0.07	
Catechin Solution	C1s	284.44 ± 0.01	35.5 ± 0.1	1.30 ± 0.02	C–H
		286.35 ± 0.01	52.0 ± 0.2	1.45 ± 0.03	C–OH/C–C–O–C
		287.85 ± 0.07	5.7 ± 0.1	1.1 ± 0.3	C=O
		289.1 ± 0.2	6.7 ± 0.1	1.6 ± 0.3	COOH
	O1s	531.3 ± 0.3	7.7 ± 0.2	1.6 ± 0.4	C=O
		532.88 ± 0.04	84.4 ± 0.1	1.5 ± 0.1	C–OH
		534.0 ± 0.5	7.9 ± 0.1	1.5 ± 0.4	C–O–C
Catechin AuNPs	C1s	284.69 ± 0.04	46.35 ± 0.08	1.83 ± 0.06	C–H
		286.38 ± 0.08	31.73 ± 0.02	1.3 ± 0.1	C–OH/C–C–O–C
		287.7 ± 0.2	16.7 ± 0.2	1.7 ± 1.4	C=O
		289.1 ± 0.4	5.0 ± 0.1	1.3 ± 0.5	COOH
	O1s	531.2 ± 0.3	8.8 ± 0.2	1.4 ± 0.3	C=O
		532.70 ± 0.05	90.0 ± 0.6	1.8 ± 0.3	C–OH
		534 ± 2	5.3 ± 0.2	2 ± 2*	C–O–C
Cocoa AuNPs	C1s	283.8 ± 0.2	13.5 ± 1.7	0.89 ± 0.35	C–C/C–H*
		285.01 ± 0.05	50.3 ± 0.7	1.59 ± 0.35	C–C/C–H*
		286.64 ± 0.14	18.8 ± 1.0	1.3 ± 0.7	C–OH/C–C–O–C
		287.8 ± 3.2	9.0 ± 2.4	—	C=O
		288.7 ± 1.1	8.3 ± 1.7	1.9 ± 0.6	COO^-
	O1s	531.8 ± 0.6	37.2 ± 0.5	1.7 ± 0.4	
		533.2 ± 0.8*	52 ± 10*	1.5 ± 1.5	
		533.8 *	1.0 ± 1.0*	—	

two pharmacophores: the catechol group in the B ring, the resorcinol in the A ring, and a hydroxyl group in the C ring, as shown in figure 4(S) in the supplementary materials. The only oxidable –OH groups are in the C ring. Alternately, the –OH groups in A and B rings, act as anti-oxidants and stabilize electrons throughout chinone-hydroquinone simile processes [42]. It is possible to assume that catechin groups act as reducing agents and as electron donors. By oxidation, catechins give two e^- to Gold(III) for its reduction, and at the same time, catechins loose two H^+. The –OH group of the B ring seems to be the most reactive, and after the oxidation, the oxidated –O groups bind with the bulk gold of AuNPs, creating a catechin coating as shown in figure 4(S) in the supplementary materials. This hypothesis is also supported by previous findings on polyphenols and flavonoids studies in green synthesis [43].

3.5. Synthesis and characterization of cocoa AuNPs from low percentage fatty acids powder

The combined spectroscopic and morphological analysis presented here confirmed the presence of a coating layer around the CAuNPs, providing insight into its chemical composition, i.e. flavonoids and fatty acid/protein residuals. However, when moving forward towards CAuNPs bio-functionalization, we found that this layer presents a challenge for removal. In this respect, we followed several physical and/or chemical routes, but no effect was sorted. Aware of the availability of different types of cocoa powder, with diverse concentrations of fatty acids, we repeated the synthesis using a lower-fat powder (reduced from 22% to 11%). The new AuNPs batch was then analyzed using UV–vis, DLS, AT-FTIR spectroscopy, and TEM microscopy. UV–vis spectroscopy

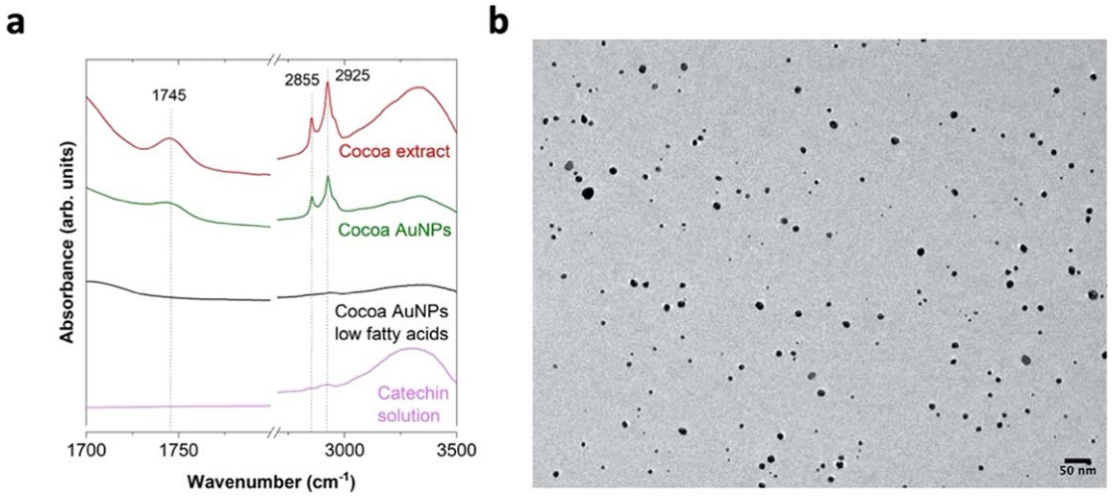

Figure 5. (a) ATR-FTIR spectrum of CAuNPs with low percentage of fatty acids (black) in the wavenumber range of 800–1800 cm^{-1} and 2700–3500 cm^{-1}. (b) Respective TEM micrograph of CAuNPs with lower content of fatty acids. Scale bar is reported.

exhibited a maximum absorption peak at 530 nm, consistent with the previous synthesis, with no significant changes in peak shape or intensity. DLS reported an average hydrodynamic diameter of 27.9 ± 9.7 nm. As previously described in the work of Kejok *et al* the values of the hydrodynamic diameter are influenced by the presence of the coating layer [32]. In fact, reducing the spot we subsequently obtained different hydrodynamic diameter values pointing out to a thinner capping layer. ATR-FTIR and TEM analyses, reported in Panel A and B of figure 5, respectively, confirmed this hypothesis. The three characteristic peaks corresponding to fatty acid residues, at 1745, 2855, and 2915 cm^{-1} respectively, are no longer present in CAuNPs (black spectrum). TEM analysis indicated that the particle core size distribution remained consistent with the one obtained previously using cocoa powder with 22% fat content, however, the new sample exhibits improved homogeneity (figure 5(b)), and the coating layer that previously caused particle aggregation is now absent. Moreover, FTIR spectra suggest that minimal protein traces may still be present.

Collectively, these results suggest that variations in fatty acids concentrations in the cocoa extract influence CAuNPs synthesis, specifically affecting nanoparticle homogeneity and presence of a coating layer. We therefore attribute the formation of the coating layer, which previously linked the particles together, primarily to fatty acids, with protein playing a minor role. Nonetheless, the role of catechins as the reducing and stabilizing agent is confirmed, as successful synthesis was achieved regardless of the content of the fatty acid content in the cacao powder.

3.6. CAuNPs passivation through mixed- SAM formation

Although the coating layer on CAuNPs was significantly reduced by using to a cocoa extract with lower fat content, it remained partially intact, as shown from the high-magnification TEM images (not reported here). Several washing procedures were adopted in attempts to remove this layer to enable biomolecule attachment to the gold surface for biomedical applications. Washing procedures including water, organic solvents such as ethanol and chloroform, and oil-based solvents were tested. However, none successfully removed the coating, and the use of the organic solvents led to aggregation. These observations point to the relevant role of the coating layer in stabilizing and protecting the AuNPs.

In particular, capitalizing on our expertise on citrate-capped AuNPs, we aimed at creating a functional SAM by mixing MUA and TOEG3 alkanethiols, by means of a simple ligand-exchange procedure, following the protocol optimized and described by Deka *et al* [44]. The MUA-TOEG3 combination enhances the stability and orientation of the functional groups (–OH end group of MUA), facilitating surface passivation (TOEG3). UV-Vis spectra of CAuNPs after functionalization attempts, reported only a slight shift (to 535 nm) for all the six concentrations of MUA:TOEG3 mix used (see figure 5(S) in the supplementary materials). Moreover, after the final centrifugation, the resuspension of the pellet was unsuccessful, forming instead dark grains. At variance, citrate-capped AuNPs demonstrated a larger redshift as the relative linker:spacer (MUA:TOEG3) concentration increased, indicating successful surface coating.

While these studies advance our understanding of the key chemical constituents in the green synthesis of AuNPs from cocoa extracts, the effective functionalization of these nanoparticles continues to be a challenge. The catechin-based coating layer, possibly enriched with proteins, impedes ligand exchange, and instead

promotes AuNP coalescence. Further investigations with alternative functionalization strategies will be necessary to exploit the functional groups that are available on CAuNPs.

4. Conclusions

In this comprehensive study, we optimized the green chemistry-based synthesis of spherical gold nanoparticles (AuNPs) through a combination of morphological and spectroscopic techniques. The synthesis parameters, including the type and quality of food extracts, the gold-to-extract ratio, and the reaction temperature were meticulously refined. Among the various extracts tested, cocoa powder emerged as the most effective, producing AuNPs with an average size of 11 nm and good dispersion. While previous studies have reported the synthesis of AuNPs using cocoa extract, our in-depth analysis provided new insights into the redox reaction steps, identifying catechins as the primary reducing agents driving the AuNP synthesis. Additionally, fatty acids and proteins present in the cocoa extract contributed to the formation of a protective layer around the AuNPs, preventing aggregation. The layer's thickness can be reduced by using cocoa powder lower fatty acid content. However, despite these optimizations, complete removal of the protective layer proved challenging, which hindered the subsequent functionalization of the AuNPs for biotechnological applications. While further investigations are required to meet the functionalization efficiency of the classical citrate-stabilized AuNPs, our findings contribute clarity to the often-inconsistent results reported in the literature regarding the green synthesis of AuNPs and lay the groundwork for future applications.

Acknowledgments

The results of this pubblication has been achieved with funding obtained under Axis IV of NOP Research and Innovation 2014-2020 "Education and research for recovery – REACT-EU", co-founded by H2020 iToBoS Grant Agreement n. 965221 (J99C21000380006).

The authors gratefully acknowledge CIMA center ('Carlo and Dirce Callerio' interdepartmental center of advanced Microscopy), especially Giovanna Baldini, Roberta Bortul, and Susanna Bossi for kindly assisting during TEM analysis. We acknowledge Diana Bedolla of the SISSI Beamline, and the Structural Biology Laboratory at Elettra Sincrotrone Trieste for technical support in sample preparation and instruments use.

Data availability statement

All data that support the findings of this study are included within the article (and any supplementary files).

Funding

The project is partially supported by 2014–2020 Research and Innovation PON founds to S.B. and C.M. and by H2020 iToBoS Grant Agreement n. 965221 (J99C21000380006) to S.B.

CRediT authorship contribution statement

Conceptualization S B, L C, P P, A A, and C M Investigation C M, A A, F D, H V, G B, D B, R C, C L C, A C, and P Po Resources L C, and S B; writing—original draft preparation, C M, A A, F D, and L C; writing— review and editing, C M, L C, P P, and S B; supervision, L C, P P, and S B; funding acquisition, L C, and S B All authors have read and agreed to the published version of the manuscript.

Declaration of competing interest

The authors declare that they have no known competing financial interests or personal relationships that could have appeared to influence the work reported in this paper.

Data availability

Data will be made available on request.

ORCID iDs

Caterina Medeot https://orcid.org/0000-0002-2880-6298
Ahmed Alsadig https://orcid.org/0000-0001-8601-7345
Francesco D'Amico https://orcid.org/0000-0001-7995-826X
Claudio Lentini Campallegio https://orcid.org/0009-0001-3629-6590
Albano Cossaro https://orcid.org/0000-0002-8429-1727
Hendrik Vondracek https://orcid.org/0000-0002-9603-4605
Pietro Parisse https://orcid.org/0000-0002-7420-2778
Loredana Casalis https://orcid.org/0000-0001-8924-4906
Serena Bonin https://orcid.org/0000-0002-7349-0296

References

[1] Govorov A O and Richardson H H 2007 Generating heat with metal nanoparticles *Nano Today* **2** 30–8
[2] Schmid G and Simon U 2005 Gold nanoparticles: assembly and electrical properties in 1–3 dimensions *Chem. Commun.* 697–710
[3] Ahmadi M, Mistry H and Roldan Cuenya B 2016 Tailoring the catalytic properties of metal nanoparticles via support interactions *J. Phys. Chem. Lett.* **7** 3519–33
[4] Finkelstein A E, Walz D T, Batista V, Mizraji M, Roisman F and Misher A 1976 Auranofin. new oral gold compound for treatment of rheumatoid arthritis *Annals of the Rheumatic Diseases* **35** 251–7
[5] Desai N, Momin M, Khan T, Gharat S, Ningthoujam R S and Omri A 2021 Metallic nanoparticles as drug delivery system for the treatment of cancer *Expert Opinion on Drug Delivery* **18** 1261–90
[6] Klębowski B, Depciuch J, Parlińska-Wojtan M and Baran J 2018 Applications of noble metal-based nanoparticles in medicine *IJMS* **19** 4031
[7] Turkevich J, Stevenson P C and Hillier J 1951 A study of the nucleation and growth processes in the synthesis of colloidal gold *Discuss. Faraday Soc.* **11** 55
[8] Deka J, Mojumdar A, Parisse P, Onesti S and Casalis L 2017 DNA-conjugated gold nanoparticles based colorimetric assay to assess helicase activity: a novel route to screen potential helicase inhibitors *Sci. Rep.* **7** 44358
[9] Aryal S, Grailer J J, Pilla S, Steeber D A and Gong S 2009 Doxorubicin conjugated gold nanoparticles as water-soluble and ph-responsive anticancer drug nanocarriers *J. Mater. Chem.* **19** 7879
[10] Ielo I, Rando G, Giacobello F, Sfameni S, Castellano A, Galletta M, Drommi D, Rosace G and Plutino M R 2021 Synthesis, chemical–physical characterization, and biomedical applications of functional gold nanoparticles: a review *Molecules* **26** 5823
[11] Nasrollahzadeh M, Sajjadi M, Sajadi S M and Issaabadi Z 2019 Green nanotechnology *Interface Science and Technology* (Elsevier) 28, 145–98
[12] Gour A and Jain N K 2019 Advances in green synthesis of nanoparticles *Artificial Cells, Nanomedicine, and Biotechnology* **47** 844–51
[13] Singh J, Dutta T, Kim K-H, Rawat M, Samddar P and Kumar P 2018 'Green' synthesis of metals and their oxide nanoparticles: applications for environmental remediation *J. Nanobiotechnol.* **16** 84
[14] Lee K X, Shameli K, Yew Y P, Teow S-Y, Jahangirian H, Rafiee-Moghaddam R and Webster T 2020 Recent developments in the facile bio-synthesis of gold nanoparticles (AuNPs) and their biomedical applications *IJN* **15** 275–300
[15] Chandran S P, Chaudhary M, Pasricha R, Ahmad A and Sastry M 2006 Synthesis of gold nanotriangles and silver nanoparticles using aloe vera plant extract *Biotechnol. Prog.* **22** 577–83
[16] Begum N A, Mondal S, Basu S, Laskar R A and Mandal D 2009 Biogenic synthesis of Au and Ag nanoparticles using aqueous solutions of black tea leaf extracts *Colloids Surf., B* **71** 113–8
[17] Srivastava S K and Constanti M 2012 Room temperature biogenic synthesis of multiple nanoparticles (Ag, Pd, Fe, Rh, Ni, Ru, Pt, Co, and Li) by pseudomonas aeruginosa SM1 *J. Nanopart. Res.* **14** 831
[18] Owais M, Chauhan A, Tufail, Sherwani, Sajid M, Suri C R and Owais M 2011 Fungus-mediated biological synthesis of gold nanoparticles: potential in detection of liver cancer *IJN* **51** 2305
[19] Chandrakala V, Aruna V and Angajala G 2022 Review on metal nanoparticles as nanocarriers: current challenges and perspectives in drug delivery systems *Emergent Mater.* **5** 1593–615
[20] Panda T and Deepa K 2011 Biosynthesis of gold nanoparticles *J. Nanosci. Nanotechnol.* **11** 10279–94
[21] Sujitha M V and Kannan S 2013 Green synthesis of gold nanoparticles using citrus fruits (citrus limon, citrus reticulata and citrus sinensis) aqueous extract and its characterization *Spectrochim. Acta, Part* A **102** 15–23
[22] Sharma R K, Gulati S and Mehta S 2012 Preparation of gold nanoparticles using tea: a green chemistry experiment *J. Chem. Educ.* **89** 1316–8
[23] Bogireddy N K R, Pal U, Gomez L M and Agarwal V 2018 Size controlled green synthesis of gold nanoparticles using *coffea arabica* seed extract and their catalytic performance in 4-nitrophenol reduction *RSC Adv.* **8** 24819–26
[24] Roy Chowdhury N, Cowin A, Zilm P and Vasilev K 2018 'Chocolate' gold nanoparticles—one pot synthesis and biocompatibility *Nanomaterials* **8** 496
[25] Kamalakannan R, Mani G, Muthusamy P, Susaimanickam A A and Kim K 2017 Caffeine-loaded gold nanoparticles conjugated with PLA-PEG-PLA copolymer for in vitro cytotoxicity and anti-inflammatory activity *J. Ind. Eng. Chem.* **51** 113–21
[26] Nadaroglu H, Ince S and Gungor A A 2017 Green synthesis of gold nanoparticles using quail egg yolk and investigation of potential application areas *Green Processing and Synthesis* **6** 43–48
[27] Choi Y 2014 Catechin-capped gold nanoparticles: green synthesis, characterization, and catalytic activity toward 4-nitrophenol reduction *Nanoscale Res Letter* **9** 103
[28] Costantini R *et al* 2018 ANCHOR-SUNDYN: a novel endstation for time resolved spectroscopy at the ALOISA beamline *J. Electron. Spectrosc. Relat. Phenom.* **229** 7–12
[29] Senigagliesi B *et al* 2022 Triple negative breast cancer-derived small extracellular vesicles as modulator of biomechanics in target cells *Nanomed. Nanotechnol. Biol. Med.* **44** 102582

[30] Thipe V C, Amiri K P, Bloebaum P, Raphael A K, Khoobchandani M, Katti K K, Jurisson S S and Katti K V 2019 Development of resveratrol-conjugated gold nanoparticles: interrelationship of increased resveratrol corona on anti-tumor efficacy against breast, pancreatic and prostate cancers *IJN* **14** 4413–28
[31] Pohjala L and Tammela P 2012 Aggregating behavior of phenolic compounds—a source of false bioassay results? *Molecules* **17** 10774–90
[32] Keijok W J, Pereira R H A, Alvarez L A C, Prado A R, da Silva A R, Ribeiro J, de Oliveira J P and Guimarães M C C 2019 Controlled biosynthesis of gold nanoparticles with coffea arabica using factorial design *Sci. Rep.* **9** 16019
[33] Grassia M 2019 Polyphenols, methylxanthines, fatty acids and minerals in cocoa beans and cocoa products *Food Measure* **13** 1721–8
[34] Soares T F and Oliveira M B P P 2022 Cocoa by-products: characterization of bioactive compounds and beneficial health effects *Molecules* **27** 1625
[35] Bhardwaj P, Kaur M, Sharma A, Singh N T, Kumar M, Katual and Kumar R 2017 Development and validation of UV spectrophotometric method for estimation of catechin in acacia catechu methanolic extract against marker compound *Development* **9** 102–108
[36] Atomssa T and Gholap A V 2015 Characterization and determination of catechins in green tea leaves using UV-visible spectrometer *JETR* **7** 22–31
[37] Aitken A and Learmonth M P 2002 Protein determination by UV absorption *The Protein Protocols Handbook* ed J M Walker (Springer Protocols Handbooks; Humana Press) 3–6
[38] Vlachos N, Skopelitis Y, Psaroudaki M, Konstantinidou V, Chatzilazarou A and Tegou E 2006 Applications of fourier transform-infrared spectroscopy to edible oils *Anal. Chim. Acta* **573–574** 459–65
[39] Cossaro A, Puppin M, Cvetko D, Kladnik G, Verdini A, Coreno M, De Simone M, Floreano L and Morgante A 2011 Tailoring SAM-on-SAM formation *J. Phys. Chem. Lett.* **2** 3124–9
[40] Barth A 2007 Infrared spectroscopy of proteins *Biochimica et Biophysica Acta (BBA) - Bioenergetics* **1767** 1073–101
[41] Rouxhet P G and Genet M J 2011 XPS analysis of bio-organic systems *Surf. Interface Anal.* **43** 1453–70
[42] Janeiro P and Oliveira Brett A M 2004 Catechin electrochemical oxidation mechanisms *Anal. Chim. Acta* **518** 109–15
[43] Latif M, Abbas S, Kormin F and Mustafa M 2019 Green synthesis of plant-mediated metal nanoparticles: the role of polyphenols *Asian J Pharm Clin Res* **12** 75–84
[44] Deka J, Měch R, Ianeselli L, Amenitsch H, Cacho-Nerin F, Parisse P and Casalis L 2015 Surface passivation improves the synthesis of highly stable and specific dna-functionalized gold nanoparticles with variable DNA density *ACS Appl. Mater. Interfaces* **7** 7033–40